ORIGINAL ARTICLE

Plasmonic colloidal nanoparticles with open eccentric cavities via acid-induced chemical transformation

Won Joon Cho[1,5], Alum Jung[2,5], Suenghoon Han[2], Sung-Min Lee[3], Taewook Kang[4], Kun-Hong Lee[2], Kyung Cheol Choi[3] and Jin Kon Kim[1]

Surface-enhanced Raman spectroscopy (SERS) has been considered a promising technique for the detection of trace molecules in biomedicine and environmental monitoring. The ideal metal nanoparticles for SERS must not only fulfill important requirements such as high near-field enhancement and a tunable far-field response but also overcome the diffusion limitation at extremely lower concentrations of a target material. Here, we introduce a novel method to produce gold nanoparticles with open eccentric cavities by selectively adapting the structure of non-plasmonic nanoparticles via acid-mediated surface replacement. Copper oxide nanoparticles with open eccentric cavities are first prepared using a microwave-irradiation-assisted surfactant-free hydrothermal reaction and are then transformed into gold nanoparticles by an acidic gold precursor while maintaining their original structure. Because of the strong near-field enhancement occurring at the mouth of the open cavities and the very rough surfaces resulting from the uniformly covered hyperbranched sharp multi-tips and the free access of SERS molecules inside of the nanoparticles without diffusion limitation, adenine, one of the four bases in DNA, in an extremely diluted aqueous solution (1.0 pM) was successfully detected with excellent reproducibility upon laser excitation with a 785-nm wavelength. The gold nanoparticles with open eccentric cavities provide a powerful platform for the detection of ultra-trace analytes in an aqueous solution within near-infrared wavelengths, which is essential for highly sensitive, reliable and direct *in vivo* analysis.
NPG Asia Materials (2015) **7**, e167; doi:10.1038/am.2015.15; published online 20 March 2015

INTRODUCTION

There is a strong demand for trace-molecule detection techniques that are simple, rapid, highly sensitive and reproducible, spanning from diagnostics in medicine to the detection of base sequence mutation. Surface-enhanced Raman spectroscopy (SERS) could be a promising candidate for extremely sensitive molecular finger-printing techniques that fulfill these technological and detection system criteria.[1]

SERS is a near-field phenomenon that relies on the intensified electric fields (E-fields) on a metal nanostructure when its localized surface plasmon resonance is excited by light.[2] These enhanced E-fields lead to a large enhancement of the Raman scattering signal.[3] Although the hot spots exhibiting these intensively localized E-fields that are usually expected between two (or multiple) noble metal nanoparticles and the sharp nanoscale tips can amplify Raman signals by $>10^6$ times for trace molecule detection,[4,5] they are not easily obtained.[6,7]

Several attempts have been made to increase the sensitivity and reproducibility for active SERS substrates. Two-dimensional arrays of various SERS-active substrates were introduced[8,9] but were not suitable for detection in solution or in an *in vivo* system because of the use of solid substrates.[10,11] To directly detect target molecules in a solution, colloidal three-dimensional (3D) SERS-active particles that could be easily dispersed in an environmental matrix, such as water, are strongly needed for label-free immunoassays and on-time biosensors.[12–15]

Some research groups fabricated Ag colloids by the aggregation of Ag nanoparticles using salt; however, the size of the aggregated colloids was highly inhomogeneous. Moreover, very small fractions ($<1\%$) of colloids are SERS-active.[13] When the size of the aggregated colloids (and thus the distance between colloids) is not uniform, the reliability of SERS becomes very poor. Thus, the preparation of uniform colloidal 3D SERS-active nanoparticles is greatly needed, and all of the colloidal nanoparticles should exhibit SERS activity.[12,16]

Furthermore, for *in vivo* detection and optical imaging, SERS-active materials should exhibit plasmonic absorption bands at near-infrared (NIR) wavelengths,[17,18] the so-called biological window (700–900 nm).[19–22] A simple approach is to use gold nanorods because the localized surface plasmon resonance peak is shifted from the visible to infrared region upon increasing the aspect ratio of the gold nanorod.[23] However, to synthesize gold nanorods with high aspect ratios,

[1]National Creative Research Center for Smart Block Copolymers, Pohang University of Science and Technology (POSTECH), Pohang, Gyungbuk, Korea; [2]Department of Chemical Engineering, Pohang University of Science and Technology (POSTECH), Pohang, Gyungbuk, Korea; [3]Department of Electrical Engineering, KAIST, Yuseong-gu, Daejeon, Korea and [4]Department of Chemical and Biomolecular Engineering, Sogang University, Seoul, Korea
[5]These authors contributed equally to this work.
Correspondence: Professor JK Kim, Department of Chemical Engineering, Pohang University of Science and Technology (POSTECH), San 31, hyo-ja dong, Pohang, Kyungbuk 790-784, Korea.
E-mail: jkkim@postech.ac.kr

2

surfactants with long alkyl chains, for example, cetyl-trimethyl-ammonium-bromide, must be used. However, because of these long chains, the analytes cannot easily contact the surface of gold (or SERS-active) nanoparticles, which results in a very low SERS signal.[24]

Halas and Nordlander and coworkers[25–28] prepared noble metals with cavities to utilize the far-field optical properties in the NIR region. One of interesting nanostructures is a nanoshell, where a spherical dielectric core is surrounded by a concentric metal shell. Although this structure changes plasmon resonance depending on the ratio of the core radius to the shell thickness, the near-field enhancement was not large. However, a noble metal with a nanoegg structure, where the center of the inner dielectric core is eccentrically located with respect to the center of the outer shell surface, exhibits significantly higher near-field enhancements at the narrowest region of the shell thickness.[27,28] To prepare a nanoegg structure, a poly(4-vinylpyridine)-immobilized substrate should be used, which results in poor dispersion of nanoparticles in aqueous solution. In addition, because the core in both the nanoshell and nanoegg structure is isolated from the environment, the accessibility (or diffusion) of SERS-active molecules to the location providing strong E-fields is limited.

Here, we introduce a novel method to prepare surfactant-free colloidal plasmonic nanoparticles with open eccentric cavities. This approach consists of a microwave-irradiation-assisted hydrothermal reaction of copper oxide (CuO) followed by replacement with gold. The hydrothermal process with microwave irradiation is very effective for producing metal nanoparticles with very rough surfaces, similar to hyperbranched sharp multi-tips because of the rapid heating and low synthesis temperature.[29,30]

The fabricated 3D colloidal gold nanoparticles with open eccentric cavities exhibited very high SERS signal intensities with excellent reproducibility, which is sufficient to detect a trace amount of adenine, one of the four bases in DNA, in an aqueous solution.[31–35] The highly intense SERS signal was attributed to both the open eccentric cavity and very rough surfaces resulting from the uniformly covered hyperbranched sharp multi-tips of the colloidal gold nanoparticles. The colloidal gold nanoparticles with eccentric cavities could be used for the detection of ultra-trace analytes in aqueous solution within the NIR wavelengths (700–900 nm), which is essential for highly sensitive, reliable and direct *in vivo* analysis.

MATERIALS AND METHODS
Fabrication of colloidal gold nanoparticles with open eccentric cavities
An aqueous solution (100 ml) consisting of copper nitrate ($Cu(NO_3)_2 \cdot 3H_2O$, 1.0×10^{-3} mol, Aldrich Inc., St. Louis, MO, USA) and urea ($CO(NH_2)_2$, 1.0×10^{-1} mol, Aldrich Inc.) was prepared by mixing these solutions for 3 min at room temperature. Then, 10 ml of the solution was irradiated using a temperature-controlled microwave synthesis system (2.45 GHz, single-mode, Greenmotif, IDX, Tochigi, Japan) at 100 °C.[30] For gold replacement of CuO, 250 μl of a gold precursor solution ($HAuCl_4 \cdot 3H_2O$, 1.0×10^{-3} mol, Aldrich Inc.) was added to 10 ml of the solution containing CuO. The molar ratio of $(HAuCl_4)/(Cu(NO_3)_2)$ was 0.25.

Characterization
The morphologies of the colloidal gold nanoparticles with open eccentric cavities were investigated using field-emission scanning electron microscopy (Hitachi, S4800) (FESEM, S4800, Hitachi, Tokyo, Japan) with an instrument operating at 10 kV and high-resolution transmission electron microscopy (HR-TEM, JEOL, JEM-2100F, Tokyo, Japan) with an instrument operating at 300 kV. To prepare the samples for HR-TEM analysis, a focused ion beam (FIB, Helios NanoLab 650, Field emission and ion technology (FEI), Hillsboro, OR,

USA) was used. The selected area was milled using Ga ions and extracted by an omniprobe mounted inside of the focused ion beam chamber. After transferring the sample onto a TEM lift-out grid, the mounted sample was finally thinned to achieve an ~ 50 nm thickness to allow electron transparency. The HR-TEM was equipped with electron energy loss spectroscopy mapping with a resolution of 0.8 eV, which was used to investigate the distribution of gold and copper in the colloidal gold nanoparticles with open eccentric cavities.

The crystalline structures of the synthesized materials were determined by X-ray diffraction using a powder X-ray diffractometer (PANalytical, pw 3373/10 X'Pert, Westborough, MA, USA) with Cu Kα radiation. The working voltage and current were 40 kV and 30 mA, respectively. The 2θ angles were scanned over a range of 10°–80° at a scan rate of 0.5° per min.

Raman signal intensity was measured in a backscattering geometry using a JY LabRam HR fitted with a liquid-nitrogen-cooled charge-coupled device detector. The spectra were collected under ambient conditions mainly using a 785-nm diode laser with 250 mW irradiation on the bottom of the solution sample. The acquisition time was 10 s. The radius of the laser spot was 0.70 μm; thus, the laser spot area was $1.54 \ \mu m^2$.

The zeta potential of the nanoparticles in aqueous solution was measured using a Zetasizer (Nano ZS, Malvern Instruments, Worcestershire, UK). The surface areas of the samples were measured by recording the nitrogen adsorption–desorption isotherms at 77 K using a Micromeritics Tristar II 3020 surface area and porosity analyzer, and the isotherms were analyzed using the Brunauer–Emmett–Teller method.

The finite-difference time-domain method (FDTD, finite-difference time-domain Solutions 7.5, Lumerical Solutions Inc, Vancouver, BC, Canada) was used to calculate the near-field distributions at the excitation wavelengths of 633 and 785 nm, and 3D unit cells were designed with boundary conditions of perfectly matched layers. Here, a single particle is regarded as in free space. We used a total-field scattered-field source with a broad Gaussian frequency spectrum (150–1000 THz) to capture the Mie scattering, where a light with the electric field polarized along the y axis propagates along the x axis. The E-field pattern crosses over the particle, namely, it yields the field both outside and within the particle. The grid size was between 2 and 5 nm. Based on the calculation of the ratio of the enhanced field to the incident field, the effect of the field enhancement was investigated. Two particles were used in this study: a smooth spherical particle and a spherical particle with an open eccentric cavity. The diameter of the colloidal particles and the diameter and depth of the eccentric open cavity were 150, 65 and 30 nm, respectively.

RESULTS
Fabrication of colloidal gold nanoparticles with open eccentric cavities
A schematic of the fabrication of the colloidal gold nanoparticles with open eccentric cavities is presented in Figure 1. The details of the experimental procedures and characterization are provided in the experimental section. By microwave irradiation of an aqueous solution containing $Cu(NO_3)_2$ and $CO(NH_2)_2$ at 100 °C, the sheets of copper hydroxyl-nitrate ($Cu_2(OH)_3(NO_3)$) crystal were formed in short times (< 3 min) (step a). Then, these sheets were assembled into spherical shapes to decrease the high surface energy in the sheets (step b). With increasing irradiation time, the $Cu_2(OH)_3(NO_3)$ located near the outer surface of spheres was transformed into CuO. Because the volume of a unit cell of monoclinic crystal of $Cu_2(OH)_3(NO_3)$ is 235 Å^3, which is larger than that of CuO (81 Å^3),[36,37] volume contraction should occur during this transformation from $Cu_2(OH)_3(NO_3)$ to CuO.

Because of the use of microwave irradiation, this transformation occurs very rapidly, which causes cracks to form near the outer surface. These cracks become the source of an open cavity (step c). The detailed mechanism of the formation of the eccentric cavity is provided in Section 1 of the Supplementary Information. Upon further increasing the microwave irradiation time, the $Cu_2(OH)_3$ (NO_3) located inside the spheres is transformed into CuO, and an eccentric cavity is formed. During this process, the $CO(NH_2)_2$
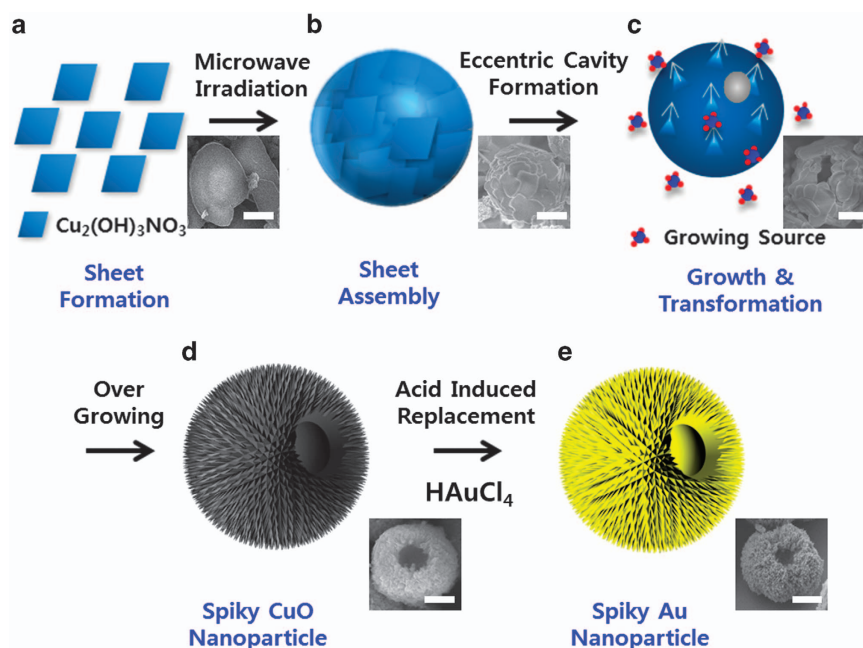
Figure 1 Scheme of the fabrication of the colloidal gold nanoparticles with open eccentric cavity. (a) Sheet formation. (b) Assembly of sheets. (c) Growth and transformation to spherical nanoparticles. (d) Spiky CuO nanoparticle with open eccentric cavity. (e) Spiky Au nanoparticle with open eccentric cavity. SEM image corresponding to each step is included (scale bar = 100 nm).

decomposition continues, which results in an increase of the concentration of hydroxyl anions (OH^-). This anion easily reacts with small amounts of Cu^{2+} and forms a complex ion, $(Cu(OH)_4)^{2-}$, which acts as a growing source for spiky or hyperbranched sharp multi-tips in the solution. After overgrowing, these tips become rapidly stabilized at the particle surface by converting into first $Cu(OH)_2$ and finally into CuO (step d).[37] We observed that the irradiation temperature becomes very crucial in the formation of an open cavity on a CuO nanoparticle. When the temperature was 95 °C, the final CuO spheres did not have open pores (Supplementary Figure S4a in the Supplementary Information). This finding might be attributed to slow heating, which could not effectively create cracks at the early stage of the transformation from $Cu_2(OH)_3(NO_3)$ to CuO. However, at 105 °C, no spherical CuO nanoparticles were produced (Supplementary Figure S4b in the Supplementary Information). This finding might be attributed to too rapid heating, which prevents the assembly of $Cu_2(OH)_3(NO_3)$ sheets into spherical form.

Finally, the surface of the colloidal CuO nanoparticles was replaced by gold through an acid-induced replacement reaction of $HAuCl_4$ in the aqueous solution at room temperature, while maintaining the original structure of CuO, followed by the reduction of $HAuCl_4$ to gold (step e). We controlled the replacement reaction of gold from CuO by changing the molar ratio of $(HAuCl_4)/(Cu(NO_3)_2)$ in the solution. From UV-Vis absorption spectra and the morphology of the nanoparticles prepared at various molar ratios, we observed that the best molar ratio for the formation of open eccentric cavities and the replacement reaction is 0.25 (see Section 7 in the Supplementary Information). Although a direct transformation of CuO to gold is an unfavorable reaction, this transforming reaction occurred when the acidic gold precursor of $HAuCl_4$ was used. Using the acid-induced replacement reaction, we obtained gold nanoparticles from other structures of CuO in candy-like or walnut-like nanoparticle forms, while maintaining the original structure. Of course, when non-acidic gold precursors (for instance, $AuCl_3$ and $Au(OH)_3$) were used, the replacement reaction did not occur (see Section 2 in the Supplementary Information).

Morphology

Figure 2 shows the morphology and inner structure of the colloidal gold particles with eccentric cavities investigated by field-emission scanning electron microscopy and electron energy loss spectroscopy mapping. The details of the sample preparation for field-emission scanning electron microscopy and HR-TEM are given in Section 3 of the Supplementary Information. The colloidal gold nanoparticles clearly contain an open cavity and have very rough surfaces resulting from the uniformly covered hyperbranched sharp multi-tips (Figures 2a and b). Notably, the open cavity is eccentric in shape, as confirmed by the field-emission scanning electron microscopy image after focus-ion beam milling (Figure 2c). The diameter of the colloidal particle was 300 ± 20 nm, and the mouth diameter and depth of the cavity were 60 ± 5 nm and 150 ± 15 nm, respectively, which were obtained by counting 150 colloidal particles.

Figure 2d presents an electron energy loss spectroscopy mapping image, where the red and yellow regions indicate CuO and gold, respectively. The inner cavity is uniformly coated by a thin layer of gold. The thickness of the gold layer (yellow region) is 47 ± 5 nm, which is consistent with that measured in the HR-TEM image (Supplementary Figure S10). The above results indicate that the size and roughness of the nanoparticle and open eccentric cavity in CuO remain the same even after the replacement of gold.

To verify the stability and surface charge of the colloidal nanoparticles, the zeta potential of the nanoparticles in aqueous solution was measured and was determined to be -41 mV at 25 °C (Figure 2e). This negative value may result from the abundant Cl^- ions and indicates that the nanoparticles are stable in aqueous solution.[38,39] For more than 1 month, the solution was very stable. The surface area of the gold nanoparticles with eccentric cavities by measured by N_2 absorption–desorption isotherm Brunauer–Emmett–Teller method) was $71.2 m^2 g^{-1}$ (Section 4 of the Supplementary Information). For
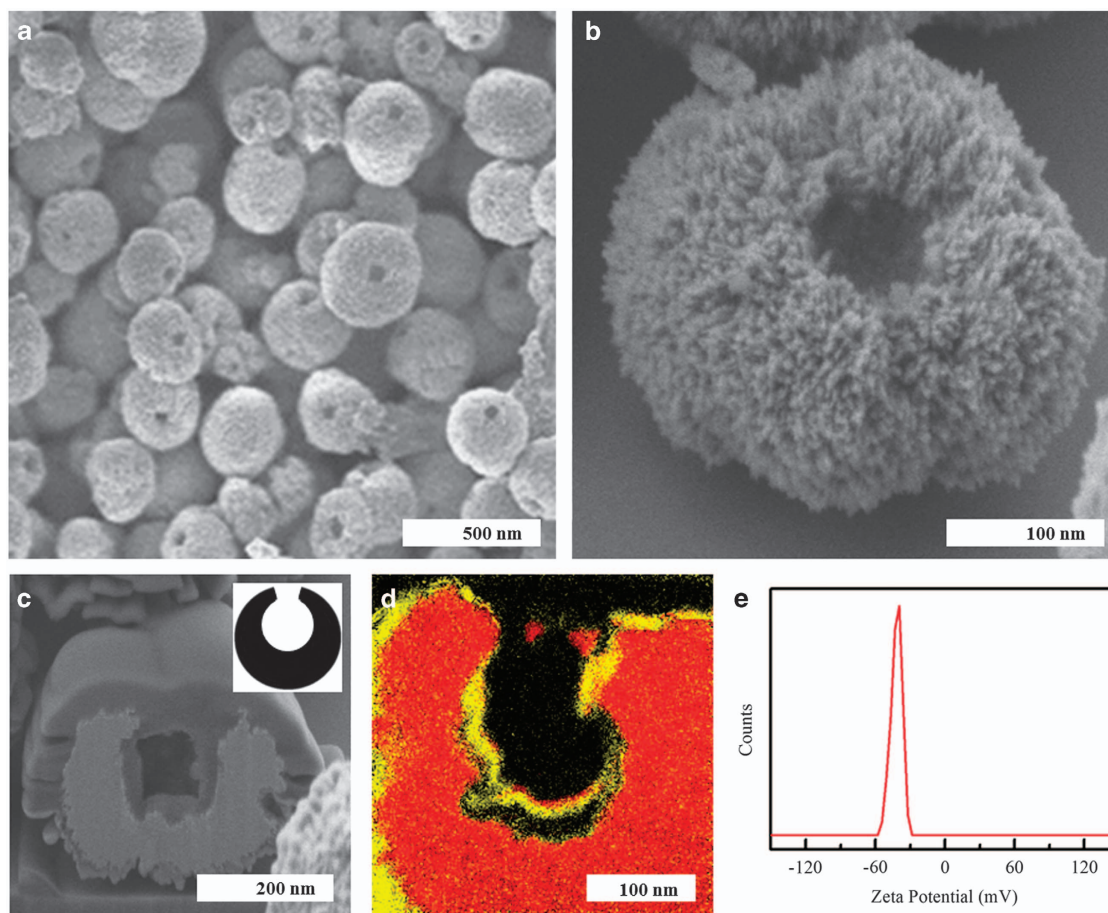
Figure 2 Morphology and inner structure of gold nanoparticles with eccentric cavity. (**a**) SEM image of gold nanoparticles with open eccentric cavity. (**b**) Enlarged SEM image of one single gold nanoparticle with open eccentric cavity. (**c**) Cross-sectional SEM image after FIB milling. (**d**) EELS mapping of (**c**). Yellow and red regions indicate gold and CuO, respectively. (**e**) Zeta potential of the colloidal gold nanoparticles with open eccentric cavity in aqueous solution.

a smooth gold nanoparticle with eccentric cavity (the diameter of the particle = 300 nm, and the diameter and depth of the cavity were 60 and 150 nm, respectively), the surface area was calculated to be only $4.0 \, m^2 \, g^{-1}$. Thus, the gold nanoparticles fabricated in this study have extremely large surface areas, which also contribute greatly to the enhancement of E-fields.[40] Furthermore, because the gold nanoparticles with eccentric cavities are prepared using a surfactant-free technique, the analytes could directly access the hot spots. Therefore, both the eccentric open cavity and rough surface would produce a very intense signal of Raman scattering even in a very dilute aqueous solution.

Optical properties and SERS analysis in aqueous solution
We investigated the optical properties and SERS effects of the colloidal gold nanoparticles with open eccentric cavities in aqueous solution. In the localized surface plasmon resonance absorption spectra, the spherical gold nanoparticles without cavities exhibit a single peak at 601 nm, whereas the colloidal gold nanoparticles with open eccentric cavities exhibit two distinct peaks at 598 and 779 nm, respectively (Figure 3a). The peak at 598 nm arises from the spherical shape of the gold nanoparticles. A new peak at 779 nm, which lies within the NIR region, results from the open eccentric cavities of the colloidal gold nanoparticles. We obtained the SERS signals of an adenine molecule $(10^{-9} \, M)$ in aqueous solution after a laser with a wavelength of

785 nm was illuminated on the colloidal gold nanoparticles with open eccentric cavities and on spherical gold nanoparticles without cavities (Figure 3b). The SERS signal intensities at both $737 \, cm^{-1}$ (the ring breathing mode) and $1333 \, cm^{-1}$ (N–C stretching mode[31]) were very large for the colloidal gold nanoparticles with open eccentric cavities. Although a narrow and single absorption peak might be ideal for SERS activity, the SERS signal intensity of the colloidal gold nanoparticles with open eccentric cavities for the two absorption peaks were 17 times higher than that of the spherical gold nanoparticles without cavities, which exhibited a single absorption peak, even though the latter sample also had a rough surface area $(69.1 \, m^2 \, g^{-1})$, very similar to that $(71.2 \, m^2 \, g^{-1})$ of the colloidal gold nanoparticles with open eccentric cavities (see Section 4 in the Supplementary Information). Thus, the large increase of the SERS signal intensity observed in Figure 3b for the colloidal gold nanoparticles with open eccentric cavities is due to the existence of open eccentric cavities.

The SERS signal is clearly detected even at an extremely diluted concentration of adenine (1.0 pM) (Figure 3c). The calculated enhancement factors and their s.d.s are shown in Figure 3d. The details of the enhancement factor calculation are provided in Section 5 of the Supplementary Information. Because the number of nanoparticles in the laser-irradiated volume was calculated to be as high as 4.8×10^2 (see Section 5 in the Supplementary Information), excellent reproducibility of the SERS signal is obtained.[13] The average
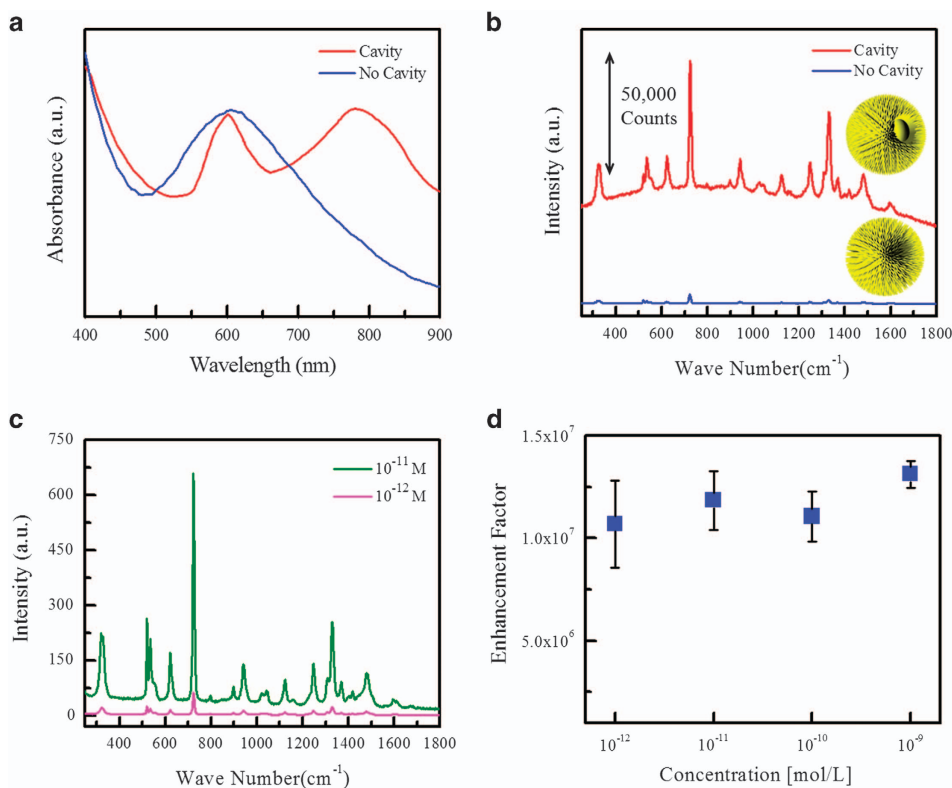
Figure 3 (a) UV-vis absorption spectra of the colloidal gold nanoparticles with open eccentric cavity and simply spherical (no cavity) gold nanoparticles in aqueous solution. (b) SERS spectra of the colloidal gold nanoparticles with open eccentric cavity and simply spherical (no cavity) gold nanoparticles with 1×10^{-9} M adenine aqueous solution. (c) SERS spectra and (d) the enhancement factors of the colloidal gold nanoparticle with open eccentric cavity at various concentrations of adenine in aqueous solution.

enhancement factors are at least 1.1×10^7, and the s.d. is <10%. The high sensitivity and excellent reproducibility are attributed to the uniform size distribution of the nanoparticles and the ensemble average effect of the numerous colloidal gold nanoparticles with open eccentric cavities. A similar SERS intensity and similar enhancement factors were obtained for crystal violet, one of the prominent SERS molecules (Supplementary Figure S11 in the Supplementary Information).

We observed that the intensities of the UV-Vis absorption peaks, especially the peak at 779 nm, were highly dependent on the amount of $HAuCl_4$ in the aqueous solution containing CuO (or the degree of the gold replacement). The best condition for the formation of open cavity structures by the gold replacement reaction was 0.25:1.0 (mol/mol) $(HAuCl_4)/(Cu(NO_3)_2)$, as observed in Supplementary Figures S8 and S12 in the Supplementary Information. At high amounts of $HAuCl_4$ (>0.5:0.5 mol/mol), the open cavity structures were destroyed. We also observed that SERS spectra varied greatly with the amount of $HAuCl_4$, as observed in Supplementary Figure S13 for adenine and Supplementary Figure S14 for crystal violet. The largest SERS intensity of both adenine and CV was observed for the gold nanoparticles with well-defined eccentric cavities.

We also used two additional lasers excited at 633 and 514 nm to study the effect of the open eccentric cavity on the SERS intensity of adenine solution, and the results are presented in Supplementary Figure S15. At excitations at both 633 and 514 nm, the difference in the Raman signal intensity between the colloidal gold nanoparticles with open eccentric cavities and the gold nanoparticles without cavities was not large; however, the intensity was markedly reduced. Therefore,

to maximize the SERS effect in aqueous solution, coupling between the plasmonic resonance and excitation laser wavelength should be used. Because the plasmon resonance resulting from open eccentric cavity in gold nanoparticles matches well with the NIR wavelength, the detection of trace biological molecules in solution is possible.

Finite-difference time-domain simulation
To understand the large SERS intensity for the gold nanoparticles with open eccentric cavities, we used the 3D finite-difference time-domain method at an excitation wavelength of 785 nm, and the results are presented in Figure 4. The E-fields were highly localized at the gold particle surface; however, the field enhancement was maximized at the open eccentric cavity of the colloidal gold nanoparticle. The open eccentric cavity structure localizes the E-fields and couples them around the mouth of the colloidal gold nanoparticle, which provides numerous hot spots. Because the SERS enhancement factor is proportional to the fourth power of the maximum field amplitude enhancement, the enhancement factor of the local field enhancement in the colloidal gold nanoparticles with open eccentric cavities might be 2.9×10^2 times higher than that for the nanoparticles without cavities. The large increase in the SERS intensity compared with the experimental value (17 times higher) is attributed to the very rough surfaces and tiny nanoparticles (diameter of ~3 nm) in the gold shell (Supplementary Figure S10) not being considered in the simulation. These results indicate that both the existence of the open eccentric cavities and very rough surfaces contribute to the strong SERS signals. Thus, gold nanoparticles with open eccentric cavities could be used for the trace detection of biological molecules in a solution that requires
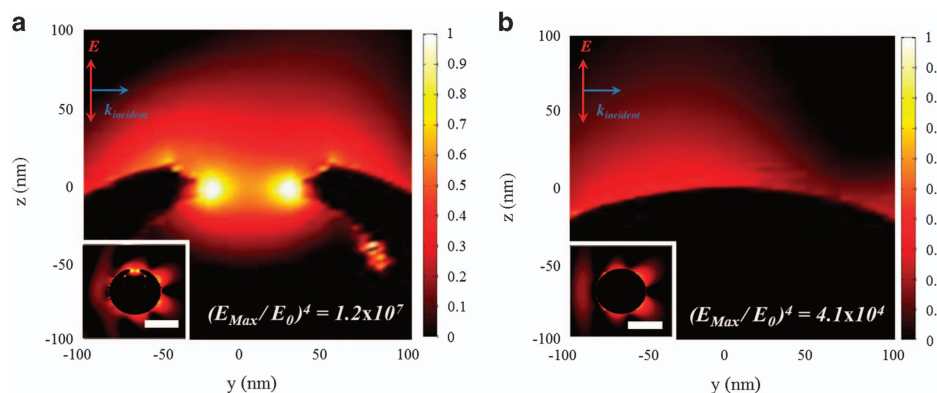
Figure 4 Three-dimensional FDTD calculation of the colloidal gold nanoparticle with open eccentric cavity and simply spherical (no cavity) gold nanoparticle at the 785 nm excitation. The E-field distribution of (**a**) the colloidal gold nanoparticle with open eccentric cavity and (**b**) simply spherical (no cavity) gold nanoparticle. Scale bar in insets is 200 nm.

NIR wavelengths, whereas gold nanoparticles without cavities could not be used.

CONCLUSIONS

We fabricated colloidal gold nanoparticles with open eccentric cavities using the microwave-irradiation-assisted surfactant-free hydrothermal reaction of CuO followed by the transformation of the nanoparticles into gold nanoparticles using an acidic gold precursor. Both the open eccentric cavity structure and very rough surfaces resulting from the uniformly covered hyperbranched sharp multi-tips in a single particle provide a powerful platform for the detection of extremely dilute analytes in an aqueous solution system at 785-nm excitation, the biological window regime, which is essential for highly sensitive, reliable and direct *in vivo* analysis. Our concept has a remarkable impact on numerous practical applications related to the large-scale production of probes for biological molecules. In addition, the results presented in this study provide a fundamental understanding of 3D plasmonic nanoparticles with broken symmetry.

CONFLICT OF INTEREST

The authors declare no conflict of interest.

1 Alvarez-Puebla, R. A. & Liz-Marzan, L. M. Traps and cages for universal SERS detection. *Chem. Soc. Rev.* **41**, 43–51 (2012).
2 Stiles, P. L., Dieringer, J. A., Shah, N. C. & Van Duyne, R. P. Surface-enhanced Raman spectroscopy. *Annu. Rev. Anal. Chem.* **1**, 601–626 (2008).
3 Etchegoin, P. G. & Le Ru, E. C. A perspective on single molecule SERS: current status and future challenges. *Phys. Chem. Chem. Phys.* **10**, 6079–6089 (2008).
4 Bosnick, K. A. & Jiang, Brus, L. E. Fluctuations and local symmetry in single-molecule Rhodamine 6G Raman scattering on silver nanocrystal aggregates. *J. Phys. Chem. B* **106**, 8096–8099 (2002).
5 Camden, J. P., Dieringer, J. A., Wang, Y., Masiello, D. J., Marks, L. D., Schatz, G. C. & Van Duyne, R. P. Probing the structure of single-molecule surface-enhanced Raman scattering hot spots. *J. Am. Chem. Soc.* **130**, 12616–12617 (2008).
6 Le Ru, E. C., Blackie, E., Meyer, M. & Etchegoin, P. G. Surface enhanced Raman scattering enhancement factors: a comprehensive Study. *J. Phys. Chem. C* **111**, 13794–13803 (2007).
7 Ueno, K. & Misawa, H. Plasmon-enhanced photocurrent generation and water oxidation from visible to near-infrared wavelengths. *NPG Asia Mater.* **5**, e61 (2013).
8 Cho, W. J., Kim, Y. & Kim, J. K. ultrahigh-density array of silver nanoclusters for sers substrate with high sensitivity and excellent reproducibility. *ACS Nano* **6**, 249–255 (2011).
9 Bae, D., Cho, W. J., Jeon, G., Byun, J. & Kim, J. K. Hierarchically well-ordered array of concentric silver nanorings for highly sensitive surface-enhanced Raman scattering substrate. *J. Phys. Chem. C* **116**, 26523–26528 (2012).
10 Qian, X. M. & Nie, S. M. Single-molecule and single-nanoparticle SERS: from fundamental mechanisms to biomedical applications. *Chem. Soc. Rev.* **37**, 912–920 (2008).
11 Feng, W., Zhu, X. & Li, F. Recent advances in the optimization and functionalization of upconversion nanomaterials for *in vivo* bioapplications. *NPG Asia Mater.* **5**, e75 (2013).
12 Jeong, E., Kim, K., Choi, I., Jeong, S., Park, Y., Lee, H., Kim, S. H., Lee, L. P., Choi, Y. & Kang, T. three-dimensional reduced-symmetry of colloidal plasmonic nanoparticles. *Nano Lett.* **12**, 2436–2440 (2012).
13 Kneipp, K., Wang, Y., Kneipp, H., Perelman, L. T., Itzkan, I., Dasari, R. R. & Feld, M. S. Single molecule detection using surface-enhanced Raman scattering (SERS). *Phys. Rev. Lett.* **78**, 1667–1670 (1997).
14 Lan, X. & Wang, Q. DNA-programmed self-assembly of photonic nanoarchitectures. *NPG Asia Mater.* **6**, e97 (2014).
15 Ma, W., Kuang, H., Xu, L., Ding, L., Xu, C., Wang, L. & Kotov, N. A. Attomolar DNA detection with chiral nanorod ssemblies. *Nat. Commun.* **4**, 2689 (2013).
16 Zrimsek, A. B., Henry, A.-I. & Van Duyne, R. P. Single molecule surface-enhanced Raman spectroscopy without nanogaps. *J. Phys. Chem. Lett.* **4**, 3206–3210 (2013).
17 Weissleder, R. A clearer vision for *in vivo* imaging. *Nat. Biotechnol.* **19**, 316–317 (2001).
18 Samanta, A., Maiti, K. K., Soh, K.-S., Liao, X., Vendrell, M., Dinish, U. S., Yun, S.-W., Bhuvaneswari, R., Kim, H., Rautela, S., Chung, J., Olivo, M. & Chang, Y.-T. Ultrasensitive near-infrared Raman reporters for sers-based *in vivo* cancer detection. *Angew. Chem. Int.* **50**, 6089–6092 (2011).
19 Zavaleta, C. L., Smith, B. R., Walton, I., Doering, W., Davis, G., Shojaei, B., Natan, M. J. & Gambhir, S. S. Multiplexed imaging of surface enhanced Raman scattering nanotags in living mice using noninvasive Raman spectroscopy. *PNAS* **106**, 13511–13516 (2009).
20 Qian, X., Peng, X.-H., Ansari, D. O., Yin-Goen, Q., Chen, G. Z., Shin, D. M., Yang, L., Young, A. N., Wang, M. D. & Nie, S. *In vivo* tumor targeting and spectroscopic detection with surface-enhanced Raman nanoparticle tags. *Nat. Biotechnol.* **26**, 83–90 (2008).
21 Wang, Y., Seebald, J. L., Szeto, D. P. & Irudayaraj, J. Biocompatibility and biodistribution of surface-enhanced Raman Scattering nanoprobes in zebrafish embryos: *in vivo* and multiplex imaging. *ACS Nano* **4**, 4039–4053 (2010).
22 Zhang, J. Z. Biomedical applications of shape-controlled plasmonic nanostructure: a case study of hollow gold nanospheres for photothermal ablation therapy of cancer. *J. Phys. Chem. Lett.* **1**, 686–695 (2010).
23 Chang, S.-S., Shih, C.-W., Chen, C.-D., Lai, W.-C & Wang, C. R. C. The shape transition of gold nanorods. *Langmuir* **15**, 701–709 (1998).
24 Biswas, S., Duan, J., Nepal, D., Pachter, R. & Vaia, R. Plasmonic resonances in self-assembled reduced symmetry gold nanorod structures. *Nano Lett.* **13**, 2220–2225 (2013).
25 Oldenburg, S. J., Jackson, J. B., Westcott, S. L. & Halas, N. J. Infrared extinction properties of gold nanoshells. *App. Phys. Lett.* **75**, 2897–2899 (1999).
26 Prodan, E., Lee, A. & Nordlander, P. The effect of a dielectric core and embeding medium on the polarizability of metallic nanoshells. *Chem. Phys. Lett.* **360**, 325–332 (2002).
27 Wang, H., Wu, Y., Lassiter, B., Nehl, C. L., Hafner, J. H., Nordlander, P. & Hallas, N. J. Symmetry breaking in individual plasmonic nanoparticles. *PNAS* **103**, 10856–10860 (2006).

28 Wu, Y. & Nordlander, P. Plasmon hybridization in nanoshells with a nonconcentric core. *J. Chem. Phys.* **125**, 1247081-10 (2006).

29 Dallinger, D. & Kappe, C. O. Microwave-assisted synthesis in water as solvent. *Chem. Rev.* **107**, 2563–2591 (2007).

30 Jung, A., Cho, S., Cho, W. & Lee, K.-H. Morphology-controlled synthesis of CuO nano- and microparticles using microwave irradiation. *Korean J. Chem. Eng.* **29**, 243–248 (2012).

31 Monica, P., Monica, B., Cosmin, F. & Simion, A. Chitosan-coated anisotropic silver nanoparticles as a SERS substrate for single-molecule detection. *Nanotech.* **23**, 055501 (2012).

32 March, J. C. & Bentley, W. E. Quorum sensing and bacterial cross-talk in biotechnology. *Curr. Opin. Biotechnol.* **15**, 495–502 (2004).

33 Lim, D., Jeon, K., Kim, H. M., Nam, J. & Suh, Y. D. Nanogap-engineerable Raman-active nanodumbbells for single-molecule detection. *Nat. Mater.* **9**, 60–67 (2010).

34 Liu, H., Zhang, L., Lang, X., Yamaguchi, Y., Iwasaki, H., Inouye, Y., Xue, Q. & Chen, M. Single molecule detection from a large-scale SERS-active Au79Ag21 substrate. *Sci. Rep.* **1**, 112 (2011).

35 Barhoumi, A. & Halas, N. J. Detecting chemically modified DNA bases using surface-enhanced Raman spectroscopy. *J. Phys. Chem. Lett.* **2**, 3118–3123 (2011).

36 Henrist, C., Traina, K., Hubert, C., Toussaint, G., Rulmont, A. & Cloots, R. Study of the morphology of copper hydroxynitrate nanoplatelets obtained by controlled double jet precipitation and urea hydrolysis. *J. Cryst. Growth* **254**, 176–187 (2003).

37 Cudennec, Y. & Lecerf, A. The transformation of Cu(OH)2 into CuO, revisited. *Solid State Sci.* **5**, 1471–1474 (2003).

38 Greenwood, R. & Kendall, K. Selection of suitable dispersants for aqueous suspensions of zirconia and titania powders using acoustophoresis. *J. Eur. Ceram. Soc.* **19**, 479–488 (1999).

39 Hanaor, D.A.H., Michelazzi, M., Leonelli, C. & Sorrell, C.C. The effects of carboxylic acids on the aqueous dispersion and electrophoretic deposition of ZrO2. *J. Eur. Ceram. Soc.* **32**, 235–244 (2012).

40 Fang, J., Du, S., Lebedkin, S., Li, Z., Kruk, R., Kappes, M. & Hahn, H. Gold mesostructures with tailored surface topography and their self-assembly arrays for surface-enhanced Raman spectroscopy. *Nano Lett.* **10**, 5006–5013 (2010).

Supplementary Information accompanies the paper on the NPG Asia Materials website (http://www.nature.com/am)